Green Chemistry

Accepted Manuscript

ROYAL SOCIETY OF CHEMISTRY

www.rsc.org/greenchem

Ethanol Conversion into Butadiene over Zr-containing Molecular Sieves doped with Silver

Vitaly L. Sushkevich[a], Irina I. Ivanova[a,b*] and Esben Taarning[c]

[a] *Department of Chemistry, Lomonosov Moscow State University, Leninskye Gory 1, bld. 3, 119991 Moscow, Russia*

[b] *A.V. Topchiev Institute of Petrochemical Synthesis, Russian Academy of Science, Leninskiy prospect, 29, 119991 Moscow, Russia*

[c] *Haldor Topsøe A/S, Nymoellevej 55 2800 Kgs. Lyngby, Denmark*

Abstract

Synthesis of butadiene-1,3 from ethanol has been studied over silver doped (1 wt%) Zr-containing molecular sieves ZrBEA, ZrMCM-41 and ZrO_2 supported on silica. The catalysts were characterized by X-ray diffraction, nitrogen adsorption-desorption, X-ray photoelectron spectroscopy, ^{29}Si MAS NMR, SEM/EDX, TEM and FTIR of adsorbed CD_3CN. The activity of the catalysts was found to increase in the following range: $Ag/ZrO_2/SiO_2$ < Ag/ZrMCM-41 < Ag/ZrBEA. This activity range correlated with the content of Lewis acid sites in the catalysts determined by FTIR of adsorbed CD_3CN. The best catalyst performance in terms of butadiene yield was observed over ZrBEA (Si/Zr = 100) promoted with silver, which showed butadiene selectivity of 56% at ethanol conversion of 48%.

Keywords: ZrBEA, ZrMCM-41, butadiene synthesis, domino reaction, Ag-promoted catalysts, FTIR of acetonitrile

---

**Corresponding author: Tel.: +7(495)939-3570; Fax: +7(495)939-3570; E-mail address: iiivanova@phys.chem.msu.ru.*

1. Introduction

Butadiene is among the most important building blocks for the production of wide variety of synthetic rubbers, elastomers and resins. Two routes are mainly pursued for its industrial synthesis: isolation from naphtha steam cracker fractions of paraffinic hydrocarbons or the catalytic and oxidative dehydrogenation of n-butane and n-butene [1]. The first route is the most important, accounting for over 95% of worldwide butadiene production [2]. But the increased production of shale gas, which contains substantial amounts of ethane, has led to a shift in the feedstock for steam crackers This circumstance will cause the shortage of the longer-chain hydrocarbons such as butadiene in the nearest future. Therefore the development of an alternative cheap and sustainable process for butadiene synthesis from biomass feedstocks is highly desirable.

One of the most perspective sources for butadiene production is ethanol, which can be produced from carbohydrate biomass. The one-step catalytic process to produce butadiene from ethanol was developed by Lebedev [3,4] and commercialized in USSR in the beginning of 1920s. Later on, Carbide and Carbon Chemicals Corporation commercialized in USA a two-step process [5-7] based on Ostromislenskiy reaction [8]. However after 1960s both processes became economically unfavorable and were stopped because butadiene was very efficiently produced from petrochemical sources.

Nowadays the interest to the technology of on-purpose butadiene production from ethanol is growing again. Recent studies [9, 10] have demonstrated that the bio-based process could be a promising substitute for the dominant naphtha-based method. However, although significant achievements have been made towards fundamental understanding of the process and the development of novel efficient catalysts during the last few years [11-19], the recent reviews [11, 12] point that there is still an ample room for catalyst improvement.

One of the most efficient ways for catalysts design and improvement involves the determination of the key reaction steps leading to the target product, the selection of the

optimum catalyst components for each reaction step, merging these components into one multifunctional catalyst and balancing their functions to achieve the highest activity and selectivity to the target product. Our recent kinetic studies over metal containing oxide catalysts [13] pointed that among the five reaction steps, which constitute the target reaction pathway leading to butadiene (Scheme 1 [11-14, 19]), steps 1,2 and 4, namely, ethanol dehydrogenation, acetaldehyde condensation and Meerwein–Ponndorf–Verley–Oppenauer (MPVO) reduction of crotonaldehyde with ethanol can be considered as the key reaction steps. Dehydration of 3-hydroxybutanal and crotyl alcohol was shown to proceed very easy, even on the weak acid sites of silica support [13]. The investigation of the key reaction steps [20-22] suggested that Ag-containing metal sites are very efficient in ethanol dehydrogenation [20], whereas Zr-containing Lewis acid sites proved to be very active and selective in aldol condensation of acetaldehyde [21] and MPVO reaction of crotonaldehyde with ethanol [22]. The interplay between the metal promoter and the acidic sites has been addressed in [13, 20]. In this paper we aimed to elucidate the effect of different Zr-containg Lewis sites, keeping the same the type and the content of metal promoter (1 wt% Ag). For this purpose, Zr-containing molecular sieves, which proved to be very active in MPVO reaction [22] have been synthesized and investigated in the overall reaction. The results are compared with Ag/ ZrO_2/SiO_2 studied in the previous work [13]. This paper is the first report on the catalytic properties of Ag-promoted ZrBEA and ZrMCM-41 molecular sieves in the ethanol conversion into butadiene.

2. Experimental

2.1 Catalysts preparation

ZrBEA zeolites with Si/Zr ratio within 100 - 400 were synthesized using the procedure, described in [23]. ZrMCM-41 was prepared by modified procedure proposed by Li et al. [24] in particular, tin chloride pentahydrate ($SnCl_4 \cdot 5H_2O$) was replaced by zirconyl chloride octrahydrate ($ZrOCl_2 \cdot 8H_2O$). The molar composition of the gel for the synthesis of ZrMCM-41 was 1Si: 0.005Zr : 0,35CTABr : 0,21TMA : 0,07Cl^- : 31,5 H_2O. The hydrothermal synthesis was

carried out at 413K for 15 hours. The sample was recovered by filtration, washed with ample water, dried overnight at 353K and calcined at 893K for 5 hours in a flow of air.

ZrO_2/SiO_2 catalyst was prepared by incipient wetness impregnation of silica gel (Karpov chemical plant) with an aqueous solution of zirconyl nitrate to attain ZrO_2 content of ~1.0 wt %. After impregnation the catalyst was dried at 393 K and calcined at 773 K for 3 h in a flow of air.

All the catalysts were modified with 1 wt% of silver by incipient wetness impregnation with $AgNO_3$ solution followed by calcination of reduction. Elemental analysis confirmed the silver content within 1.1-0.9 wt%.

The molecular sieves samples were assigned as ZrSieve_type(x), were x is Si/Zr ratio. The catalysts promoted with silver were labeled as Ag/ZrSieve_type(x) or $Ag/ZrO_2/SiO_2$.

2.2 Catalysts characterization

The elemental analysis was performed using inductively coupled plasma atomic emission spectroscopy (ICP-AES). Prior to the analysis the samples were dissolved in a mixture of HF, HCl, HNO_3 and H_3PO_4, followed by the neutralization with $B(OH)_3$. The solution was analyzed using a Perkin Elmer Optima 3000 (Varian Vista). N_2 sorption-desorption isotherms were measured at 77K using a Quantachrome Autosorb automatic surface area and pore size analyzer.

Powder x-ray diffraction (XRD) patterns of the samples were obtained on a Phillips X'Pert Diffratometer using Cu-K(alpha) radiation at a wavelength of 1,5456 Å.

TEM images were obtained using JEOL JEM 2010 electron microscope operating at 200 kV. SEM/EDX analysis was performed using Oxford Instruments MIRA3 TESCAN microscope.

XPS spectra were collected on an Axis Ultra DLD (Kratos Analysis) spectrometer using an Al Kα X-ray source. Due to the charging of the insulating samples, the binding-energy values were referenced to the C 1s line at 284.5 eV (arising from the inadvertent carbon contamination).

^{29}Si solid-state MAS NMR was performed using a Bruker Avance-400 spectrometer, operating at a resonance frequency of 79.46 MHz with a spinning rate of 10 kHz, pulse length of 3 μs, and recycle time of 20 s. The ^{29}Si chemical shifts are reported relative to TMS.

The acidic properties were studied by FTIR spectroscopy of adsorbed CD_3CN. IR spectra were recorded with a Nicolet Protégé 380 FT-IR spectrometer at a 4 cm^{-1} optical resolution. Prior to the measurements, the catalysts were pressed in self-supporting discs and activated in the IR cell attached to a vacuum line at 723K for 4h. Adsorption of CD_3CN was carried out in the room temperature cell. The pressure was measured by a Barocell gauge. Difference spectra were obtained by the subtraction of the spectra of the activated catalyst samples from the spectra of the samples with adsorbate. The subtraction was carried out using OMNIC 7.3 package.

2.3 Catalysts evaluation

Catalytic experiments were carried out in a flow-type fixed-bed reactor under atmospheric pressure. In a typical experiment, 2 g of catalyst (fraction 0.5-1 mm) was packed into the quartz tubular reactor and purged with nitrogen at 873K for 0.5 h. Ethanol (95 wt%) was used as a feed. The reaction mixture was fed using Razel syringe pump. Helium was used as a carrier gas (molar ratio EtOH/He = 1). The WHSV was varied from 0.12 to 0.64 h^{-1}, the reaction temperature was 600K. Gaseous products were analyzed on line on Crystal 2000M gas chromatograph using 50m SE-30 column. Liquid products were separated and analyzed using 50m SE-30 and 2m Porapak Q columns. Methane was used as an external standard for gaseous products.

The conversion of ethanol, selectivity towards products and yields were calculated as follows:

$$\text{Ethanol conversion} = \frac{m_{reacted\,(EtOH)}}{m_{fed\,(EtOH)}} \cdot 100\%$$

$$\text{Selectivity} = \frac{k_j^F \dfrac{m_j}{Mr_j} \cdot 100\%}{m_{reacted\,(\mathrm{EtOH})} / 46}$$

$$\text{Yield} = \text{Ethanol conversion} \cdot \text{Selectivity}/100\,,$$

where m_j – mass of j-product in reaction mixture, Mr_j – molecular weight of j-product, k^F_j – number of ethanol molecules required for product j formation.

3. Results and discussion

3.1. Catalysts structure and composition

The chemical and textural characteristics of the catalysts precursors are presented in Table 1. The amount of ZrO_2 incorporated into ZrBEA, ZrMCM-41 and loaded onto silica is close to the expected values.

Nitrogen adsorption-desorption data point to very high surface area of zeolitic and mesoporous catalysts (Table 1). ZrBEA(200) has reversible Type-I adsorption/desorption isotherm with a steep rise at $p/p_0 < 0.01$, typical for microporous solids (Fig. 1). Similar isotherms are observed for ZrBEA catalysts with different Si/Zr ratio (not shown on Fig.1). ZrMCM-41 material shows Type-IV isotherm with a step at $p/p_0 \sim 0.35$, corresponding to the uniformly sized mesopores of ca. 35 Å in diameter. The silica supported ZrO_2 reveals surface areas of 270 m^2/g and the average pore sizes of ~100 Å, typical for amorphous silica gels.

The structure of the catalysts was analyzed by XRD techniques (Fig. 2). The powder XRD patterns of ZrBEA(200) sample show typical features of well-crystalline zeolites. For ZrBEA the asymmetry of the peak in the range of $2\theta = 7^\circ–9^\circ$ indicates the presence of two isostructures, polymorphs A and B [23]. No peaks due to crystalline ZrO_2 or any other crystalline impurity phases are detected. ZrBEA samples with Si/Zr = 200 and 400 (not presented in Fig 2) do not show any differences with respect to ZrBEA(200). The low angle XRD patterns of ZrMCM-41 show one major (100) reflection and two minor reflections corresponding to the (110) and (220) planes, pointing to a highly ordered hexagonal pore structure. ZrO_2/SiO_2 catalyst exhibits XRD patterns typical for amorphous materials (Fig. 2).

The local structure of Zr and the incorporation of Zr into the silica frameworks were studied using XPS and ^{29}Si MAS NMR techniques. The photoelectron peaks for Zr 3d observed over ZrBEA, ZrMCM-41 and ZrO_2/SiO_2 samples are shown in Fig. 3. The binding energy of $Zr3d_{5/2}$ (182.9 eV) observed for these samples is significantly higher than that of bulk ZrO_2 (182.2 eV) [23, 25]. This shift towards higher values can be due to the formation of Si-O-Zr

bonds, i.e. the incorporation of Zr into the framework of zeolites, MCM-41 or silica [26]. The higher binding energy of Zr 3d indicates a higher positive charge on the Zr incorporated in silica framework due to the lower electronegativity of Zr than that of Si. These observations are in line with the results, previously reported for ZrBEA [26], ZrMFI [27] and ZrO_2/SiO_2 [25].

Fig. 3 displays the ^{29}Si MAS NMR spectra for Zr-containing materials. ZrBEA(200) shows resonances in the range of -110 to -120 ppm typical for Q^4 species. These signals can be assigned to Si(4Si) sites located in different crystallographic positions of zeolite BEA. The spectrum shows a relatively complex feature due to the superposition of several resonances for nonequivalent T crystallographic sites in BEA (9 sites), which are not resolved. The lack of resolution can be accounted for by the presence of Zr, which induces distortion of the lattice. No Q^3-resonance indicative of Si(OH, 3Si) structural defects are observed, which confirms the high quality of ZrBEA material used for this study.

The spectrum observed for ZrMCM-41 is typical for MCM-41 and other amorphous silicas, which do not have short range ordering. The signal at ca. -108.5 ppm is due to Q^4 (Si(4Si)) species and a shoulder at ca. -100 ppm points to the presence of Q^3 (Si(OH, 3Si)) defects [28]. The ^{29}Si MAS NMR spectrum of ZrO_2/SiO_2 is very similar to those observed for ZrMCM-41, pointing to the same local structure of siliceous species in these samples.

The analysis of the XPS and ^{29}Si MAS NMR data suggests that Zr is incorporated in the frameworks of zeolite and MCM-41 materials. In the case of ZrO_2/SiO_2 catalyst the formation of Si-O-Zr bonds is also evident. However due to the impregnation procedure used, these species are most probably located on the surface of silica and the formation of tiny zirconia islands on the silica surface is more probabale than the incorporation of isolated zirconium atoms.

The Ag promoter supported over different catalysts has been characterized using SEM/EDX and TEM techniques. The images are shown in Figs. 6, 7 for the Ag/BEA(100) sample. The results point to rather uniform distribution of Ag particles of 2-5 nm size over the

catalyst. Such particle size was reported to be close to optimal for alcohols dehydrogenation [20, 31].

No significant difference was observed in Ag dispersion and distribution over different supports. On the contrary, the acidic properties showed significant variation.

3.2. Acidic properties

The nature of the acid sites was investigated by the FTIR spectroscopy of adsorbed deutirated acetonitrile. CD_3CN was selected for this study, since it is a well-established probe molecule for the characterization of the acidity of zeolitic, mesoporous and oxide catalysts [29]. The adsorption of CD_3CN at room temperature on acidic catalysts leads to the formation of H-bonds with OH groups and to the coordination of CO to Lewis acid sites. Due to this interaction, the ν(C≡N) vibration band of adsorbed acetonitrile shifts to higher wavenumbers with respect to the band of phisosorbed CD_3CN (2268 cm^{-1}). This shift is characteristic for the nature (Lewis or OH) and strength of the site. Application of CD_3CN as a probe molecule allows for easy access to most of the sites due to its very small size. This brings an additional advantage for the investigation of the acidity of microporous solids.

In a typical experiment, an equilibrium pressure of 0.5 torr of acetonitrile-d^3 was introduced in the IR cell and after the adsorption for 1 hour spectrum was collected. The results obtained are shown in Fig. 5. The adsorption of CD_3CN on all samples leads to the appearance of the bands at 2303 and 2275 cm^{-1} (Fig. 5). These bands can be attributed to the ν(C≡N) vibrations of CD_3CN adsorbed on the Lewis acid sites (Zr tetrahedral sites) and surface silanol groups, respectively [30]. For ZrBEA catalysts the band at 2203 cm^{-1} due to physically adsorbed CD_3CN is also observed. Evacuation of the acetonitrile at ambient temperature leads to vanishing of the bands corresponding to the adsorption of CD_3CN on silanol groups and physically adsorbed acetonitrile, which points on weak interaction with the surface and Si-OH.

For the quantification of the adsorbed CD_3CN spectra a deconvolution procedure was performed. Three Gauss-Lorentz components centered at 2303, 2275 and 2268 cm-1 with fixed

full width at half maximum (FWHM) were used for spectra fitting. The results are shown in Table 2. The area of the band corresponding to the CD_3CN adsorption on Lewis sites increases in the following order of samples: ZrO_2/SiO_2 < ZrMCM-41(200) < ZrBEA(400) < ZrBEA(200) < ZrBEA(100). Whereas the intensity of the band attributed to H-bonded acetonitrile increases as following: ZrO_2/SiO_2 < ZrBEA(100) ≈ ZrBEA(200) ≈ ZrBEA(400) << ZrMCM-41(200). These results show that ZrBEA(100) catalyst possesses the highest Lewis acidity and ZrMCM-41(200) sample has higher concentration of surface Si-OH groups in comparison with other catalyst.

The lowest content of Zr Lewis sites is observed over ZrO_2/SiO_2 catalyst. This observation can be explained by the different distribution and localization of Zr atoms in this catalyst. Indeed, in molecular sieve catalysts most part of Zr is located in the form of Zr(OSi)4 isolated species in the T-positions of the framework. On the contrary, in ZrO_2/SiO_2(200) catalyst ZrO_2 is deposited via impregnation, which usually leads to non-uniform distribution of Zr on the surface of silica with the formation of ZrO_2 aggregates along with Zr(OSi)4 species. Therefore, molecular sieves catalysts should contain more isolated Zr sites.

3.3. Catalyst evaluation in ethanol conversion into butadiene

3.3.1. Reaction products and the reaction network

The reaction products observed over the catalysts studied can be subdivided into 5 main groups shown in Fig. 8:

1) butadiene and small amounts of intermediate products leading to butadiene (Scheme 1), mainly, acetaldehyde and crotonaldehyde;
2) diethyl ether and ethylene obtained via ethanol dehydration;
3) ethyl acetate formed from acetaldehyde via Tischenko reaction and the products of its further transformation - acetone and propylene.
4) butanol-1 and butenes formed from crotyl alcohol via hydrogenation, dehydration and isomerization steps;

5) hexatrienes and other heavy products obtained by cross condensation of acetaldehyde with crotonaldehyde and other aldehydes.

The kinetics of these products formation has been studied in detail in our previous paper [13] over metal promoted oxide catalysts. It should be mentioned that Ag-promoted Zr-containing molecular sieves show the same set of products and obey the same mechanism of transformations.

3.3.2 Effect of the type of catalyst

The results on ethanol conversion over the catalysts studied are shown in Table 3. The comparison of the catalysts with the same composition and different structure point that molecular sieve catalysts Ag/ZrBEA(200) and Ag/ZrMCM-41(200) are much more active with respect to $Ag/ZrO_2/SiO_2(200)$. Since the content of Ag and the metal dispersion is similar over all the catalysts, the reason should be due to the different properties of the supports, which are governed by the state and location of Zr atoms.

Our previous studies on acetaldehyde condensation [21] and MPVO reaction of crotonaldehyde with ethanol [22] pointed to the key role of Zr^{4+} Lewis acid sites in these reaction steps. This study confirms the above conclusion for the overall reaction of ethanol conversion into butadiene. Indeed, the activity range of catalysts (Table 3) correlates with the relative amount of Lewis acid sites determined by FTIR of adsorbed CD_3CN (Fig. 5, Table 2).

The analysis of the product distribution and selectivity of the catalysts was carried out at the same conversion level of ethanol (Table 4). Similar ethanol conversions within 29-31% were achieved by variation of WHSV in the range of 0.12 – 0.64 g/g•h. The results point that Ag/ZrBEA(200), Ag/ZrMCM-41(200) and $Ag/ZrO_2/SiO_2(200)$ catalysts show very similar selectivity in the range of 65-66%. This observation suggests that Zr^{4+} sites located in molecular sieve frameworks and incorporated in amorphous silica exhibit the same selectivity in the overall reaction. However, some differences are observed in the by-product distribution (Table 4):

- Ag/ZrMCM-41(200) shows the highest content of the products of ethanol dehydration – diethyl ether and ethene, which is most probably due to the high amount of surface silanol groups over this sample, as evidenced by the FTIR spectra of adsorbed CD_3CN (Fig. 5, Table 2).
- $Ag/ZrO_2/SiO_2(200)$ catalyst shows the highest contribution of heavy by-products (14%) with respect to Ag/ZrBEA(200) (7-10%) and Ag/ZrMCM-41(200) (6%). This result can be related to the difference in the pore structure of the catalysts: zeolite BEA and MCM-41 have smaller pores than silica based catalyst (Table 1, Fig. 1) and the formation of large molecules of hexatrienes can be inhibited over these catalysts due to geometric factor.
- Ag/ZrBEA(200) provide for the highest amount of butenes on the expense of ethanol dehydration products and hexatrienes.

To assess the stability of the catalytic activity of different catalysts in the time course of the reaction, the yield of butadiene is plotted versus time on stream in Fig 9. The results show that Ag/ZrBEA(200), Ag/ZrMCM-41(200) and $Ag/ZrO_2/SiO_2(200)$ catalysts demonstrate similar deactivation patterns (Fig. 9a). It should be noted that the loss of the yield is associated with the decrease of ethanol conversion, whereas selectivity into butadiene and other by-products changes only slightly (Fig. S1). Therefore the deactivation of the catalysts studied is most probably due to the gradual poisoning of active sites by coke deposits as confirmed by TG analysis (Fig S2).

3.3.3 Effect of ZrBEA composition

To elucidate the influence of Zr content on catalyst activity, selectivity and deactivation, Ag/ZrBEA catalysts with Si/Zr ratio in the range of 100 - 400 are compared in Tables 3, 4 and Fig. 9b. The increase of Zr content leads to the significant enhancement of the ethanol conversion from 30 to 48% (Table 3) due to the increase of the content of Lewis sites responsible for this reaction (Table 2).

The analysis of the product distribution (Table 4) suggests that all Ag/ZrBEA catalysts have similar selectivity to butadiene. Slight decrease of the selectivity to butadiene and the increase of the contribution of heavier products over Ag/ZrBEA(100) can be accounted for by the higher density of Zr sites in Ag/ZrBEA(100). Thereby, the intermediate products, such as acetaldehyde or/and crotonaldehyde formed over one site, can undergo the further condensation reactions into heavier C_6+ products over the neighboring sites. The latter can be transformed into hexatrienes by the sequence of MPVO and dehydration reactions [13].

Deactivation curves over Ag/ZrBEA catalysts are compared in Fig. 9b. Ag/ZrBEA(200) and Ag/ZrBEA(400) samples show similar deactivation curves with gradual decrease of butadiene yield with time on stream. Ag/ZrBEA(100) catalyst is more stable during the first 5 hours, but afterwards it shows faster deactivation. Such deactivation behavior is typical for pore blocking mechanism. Further studies are necessary for the understanding of different deactivation behavior of Ag/ZrBEA(100) and Ag/ZrBEA(200), Ag/ZrBEA(400) catalysts.

The comparison of different Ag-promoted Zr-containing molecular sieves shows that the highest butadiene yield of 27% is achieved so far over Ag/ZrBEA(100). The comparison of this result with the literature data [11-19] points that the activity of molecular sieve catalysts is comparable with oxide based systems. Further progress in this field requires widening of the list of molecular sieve structures and optimization of the reaction conditions.

4. Conclusions

Butadiene synthesis from ethanol has been studied over a series of Ag-promoted Zr-containing catalysts including ZrBEA zeolites, ZrMCM-41 mesoporous material and zirconia supported on silica. All types of catalysts show the same set of products and obeyed the same mechanistic pathways. The main side reactions are found to involve: 1) ethanol dehydration into diethyl ether and ethylene; 2) conversion of acetaldehyde into ethyl acetate and further into acetone and propylene; 3) cross-condensation of acetaldehyde with crotonaldehyde and other

aldehydes into heavy by-products; and 4) hydrogenation of crotyl alcohol into butanol-1 followed by its dehydration and isomerization into butene-1 and butene-2.

Whereas all the catalysts demonstrate similar selectivity of ca. 65 % at the same conversion level of ca. 30%, the activity is found to change in the following order of catalysts: $Ag/ZrO_2/SiO_2(200) << Ag/ZrMCM\text{-}41(200) < Ag/ZrBEA(200)$. This activity range is due to the higher content of isolated Zr sites in molecular sieves catalysts with respect to silica supported catalysts. The increase of Zr content in Ag/ZrBEA leads to further activity enhancement. This activity range correlates with the amount of Lewis acid sites in the catalysts determined by FTIR of adsorbed CD_3CN.

The best catalyst performance in terms of butadiene yield (27%) is achieved over Ag/ZrBEA(100). On this catalyst the selectivity to butadiene is 56% at ethanol conversion of 48%.

5. References

[1] W. C. White, Chem.-Biol. Interact. 2007, 166, 10–14.

[2] J. Grub, E. Loser, Butadiene in Ullmann's Encyclopedia of Industrial Chemistry, Wiley-VCH, Weinheim 2012.

[3] S. V. Lebedev, British Patent 331402.

[4] S. V. Lebedev, J. Gen. Chem. 1933, 3, 698 – 708.

[5] W. J. Toussaint, J. T. Dunn, U. S. Patent 2,357,855, 1944.

[6] W. Toussaint, J. Dunn, D. Jackson, Ind. Eng. Chem., 1947, 39, 120 –125.

[7] B. B. Corson, H. E. Jones, C. E. Welling, J. A. Hinckley, E. E. Stahly, Ind. Eng. Chem. 1950, 42, 359 –373.

[8] J. Ostromislenskiy, J. Russ. Phys. Chem. Soc. 1915, 47, 1472 –1506

[9] A. D. Patel, K. Meesters, H. den Uil, E. de Jong, K. Bloka, M. K. Patel, Energy Environ. Sci., 2012, 5, 8430-8444

[10] J. A. Posada, A. D. Patel, A. Roes, K. Blok, A. C. Faaij, M. K. Patel, Biores. Technol., 2013, 135, 490–499

[11] C. Angelici, B. M. Weckhuysen, P. Bruijnincx, ChemSusChem, 2013, 6, 1595-1614

[12] E.V. Makshina, M. Dusselier, W. Janssens, J. Degrève, P. Jacobs, B. Sels, Chem. Soc. Rev., 2014, 43, 7917-7953.

[13] V. Sushkevich, I. Ivanova, V. Ordomsky, E. Taarning, ChemSushChem, 2014, 9, 2527-2536.

[14] C. Angelici, M.E.Z. Velthoen, B.M. Weckhuysen, P.C.A. Bruijnincx, ChemSusChem, 2014, 7, 2505-2515.

[15] E.V. Makshina, W. Janssens, B.F. Sels, P.A. Jacobs, Catal. Today, 2012, 198, 228-344.

[16] M. Jones, C. Keir, C.Di Iulio, R. Robertson, C. Williams, D. Apperley, Catal. Sci. Technol., 2011, 1, 267-272.

[17] M. Lewandowski, G.S. Babu, M. Vezzoli, M. D. Jones, R. E. Owen, D. Mattia, P. Plucinski, E. Mikolajska, A. Ochenduszko, D.C. Apperley, Cat. Comm., 2014, 49, 25-28.

[18] H.-T. Chae, T.-W. Kim, Y.-K. Moon, H.-K. Kim, K.-E. Jeong, C.-U. Kim, S.-Y. Jeong, Appl. Catal. B. Env., 2014, 150-151, 596-604.

[19] W. Janssens, E. Makshina, P. Vanelderen,. F. De Clippel, K. Houthoofd, S. Kerkhofs, J. A. Martens, P. A. Jacobs, B. F. Sels, ChemSusChem, 2014, 10.1002/cssc.201402894.

[20] V. Sushkevich, I. Ivanova, E. Taarning, ChemCatChem, 2013, 5, 2367-2373.

[21] V. Ordomsky, V. Sushkevich, I. Ivanova, J. Mol. Cat. A. Chem., 2010, 333, 85-93.

[22] V. Sushkevich, I. Ivanova, S. Tolborg, E. Taarning, J. Catal., 2014, 316, 121-129.

[23] Y.Z. Zhu, G.K. Chuah, S. Jaenicke, J. Catal., 2004, 227, 1-10.

[24] L. Li, C. Stroobants, K. Lin, P.A. Jacobs, B.F. Sels, P.P. Pescarmona, Green Chem., 2011, 13, 1175-1181.

[25] B. Zhang, M. Tang, J. Yuan, L. Wu, Chin. J. Catal., 2012, 33, 914-921

[26] S. Damyanova, L. Petrov, M.A. Centeeno, P. Grange, Appl. Catal. A, 2002, 224, 271-284.

[27] B. Rakshe, V. Ramaswamy, S.G. Hegde, R. Vetrivel, A.V. Ratnasamy, Catal. Lett. 1997, 45, 41-50.

[28] X.X. Wang, F. Lefebvre, J. Patarin, J.-M. Basset, Micropor. Mesopor. Mater.2001, 42, 269-276

[29] J. Ryczkowski, Catal. Today, 2001, 68, 263-381.

[30] M. Boronat, P. Concepcion, A. Corma, M. Renz, S. Valencia, J. Catal. 2005, 234, 111−118.

[31] K. Shimizu, K. Sugino, K. Sawabe, A. Satsuma, Chem. Eur. J. 2009, 15, 2341–2351.

Acknowledgements

The authors thank the Russian Science Foundation for the financial support (Grant №14-23-00094). Vitaly Sushkevich gratefully acknowledges Haldor Tøpsoe A/S for a PhD fellowship.

Table 1. Catalysts characteristics

Sample	Si/Zr ratio	Surface area (m^2/g)	Total pore volume (cm^3/g)	Micropore volume (cm^3/g)	Average pore diameter (Å)
ZrBEA(100)	134	470	0.29	0.20	7
ZrBEA(200)	263	470	0.30	0.20	7
ZrBEA(400)	455	465	0.30	0.20	7
ZrMCM-41(200)	184	870	1.1	-	35
ZrO_2/SiO_2(200)	195	270	0.70	-	100

Table 2. Relative intensities of the bands observed after acetonitrile-d^3 adsorption

Sample	Area of the band centered at 2303 cm-1 (Lewis sites)	Area of the band centered at 2275 cm-1 (OH groups)
ZrBEA(100)	0.97	1.27
ZrBEA(200)	0.75	1.07
ZrBEA(400)	0.69	1.26
ZrMCM-41(200)	0.66	2.08
ZrO_2/SiO_2(200)	0.42	0.92

Table 3. Ethanol conversion and products distribution over Zr catalysts (T = 593 K, WHSV = 0.32 g/g•h, TOS = 3h)

Sample	Ethanol conversion, %	Selectivity, mol %							
		Butadiene	Ethylene	Propylene	Butenes	Ethyl ether	Ethyl acetate	1-Butanol	C_6+
Ag/ZrBEA(100)	47.9	55.6	1.5	3.9	8.7	5.6	0.5	0.3	24.0
Ag/ZrBEA(200)	30.6	66.3	5.2	3.1	6.8	9.0	2.1	0.7	6.9
Ag/ZrBEA(400)	32.4	67.2	4.2	2.8	7.0	8.6	2.2	0.7	7.3
Ag/ZrMCM-41(200)	29.8	65.9	7.4	3.4	4.1	9.9	2.5	1.1	5.7
Ag/ZrO_2/SiO_2(200)	11.9	66.8	2.6	2.8	3.1	3.5	3.9	2.6	14.7

Table 4. Selectivity of Zr catalysts in ethanol conversion (T = 593 K, TOS = 3h)

Sample	Ethanol conversion, %	Selectivity, mol %								WHSV, g/g•h
		Butadiene	Ethylene	Propylene	Butenes	Ethyl ether	Ethyl acetate	1-Butanol	C_6+	
Ag/ZrBEA(100)	30.1	63.9	3.7	3.4	7.8	8.6	1.1	0.9	10.6	0.64
Ag/ZrBEA(200)	30.6	66.3	5.2	3.1	6.8	9.0	2.1	0.7	6.9	0.32
Ag/ZrBEA(400)	32.4	67.2	4.2	2.8	7.0	8.6	2.2	0.7	7.3	0.32
Ag/ZrMCM-41(200)	29.8	65.9	7.4	3.4	4.1	9.9	2.5	1.1	5.7	0.32
Ag/ZrO_2/SiO_2(200)	30.5	64.7	3.8	3.4	3.8	4.6	3.9	2.7	13.1	0.12

Figure captures

Fig. 1. Nitrogen adsorption/desorption isotherms obtained at 77 K

Fig. 2 XRD patterns of Zr-containing catalysts

Fig. 3. XPS spectra of Zr-containing catalysts

Fig. 4. ^{29}Si MAS NMR spectra of Zr-containing catalysts

Fig. 5. FTIR spectra of CD_3CN adsorbed over Zr-containing catalysts

Fig. 6. Main reactions pathways

Fig. 7. TEM images of Ag/ZrBEA(100) catalyst.

Fig. 8. SEM/EDX silver mapping of Ag/ZrBEA(100) catalyst.

Fig. 9. Yield of butadiene versus time on stream (T = 593K, WHSV = 0.32 g/g•h)

Scheme captures

Scheme 1. Main reaction pathway leading to butadiene

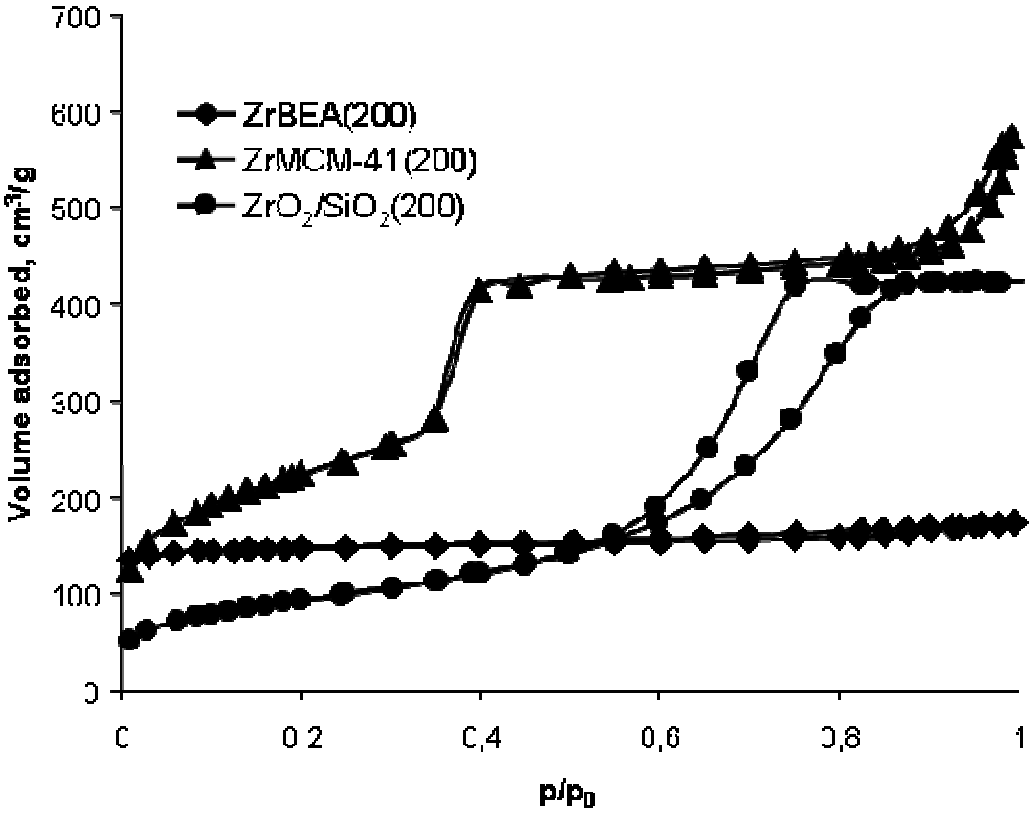

Fig. 1

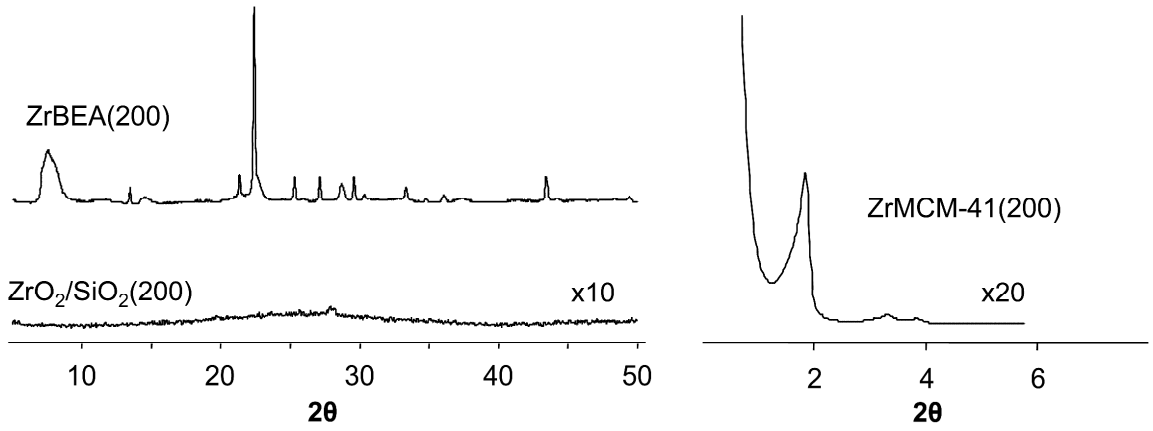

Fig. 2

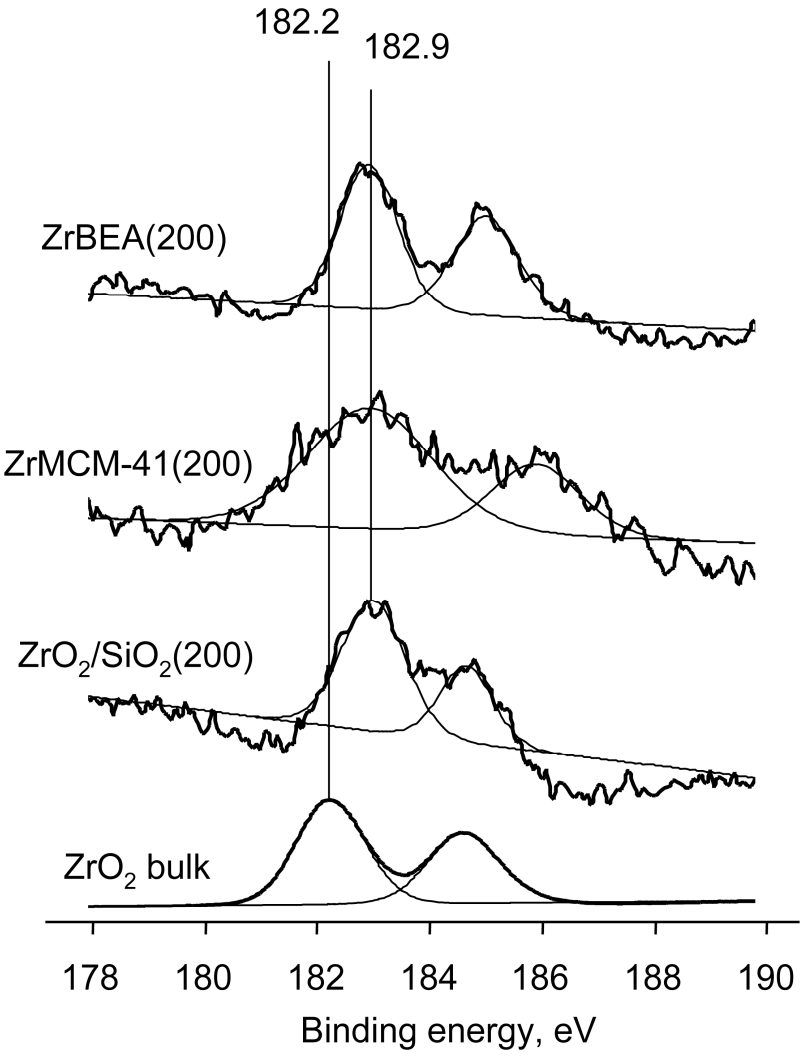

Fig. 3

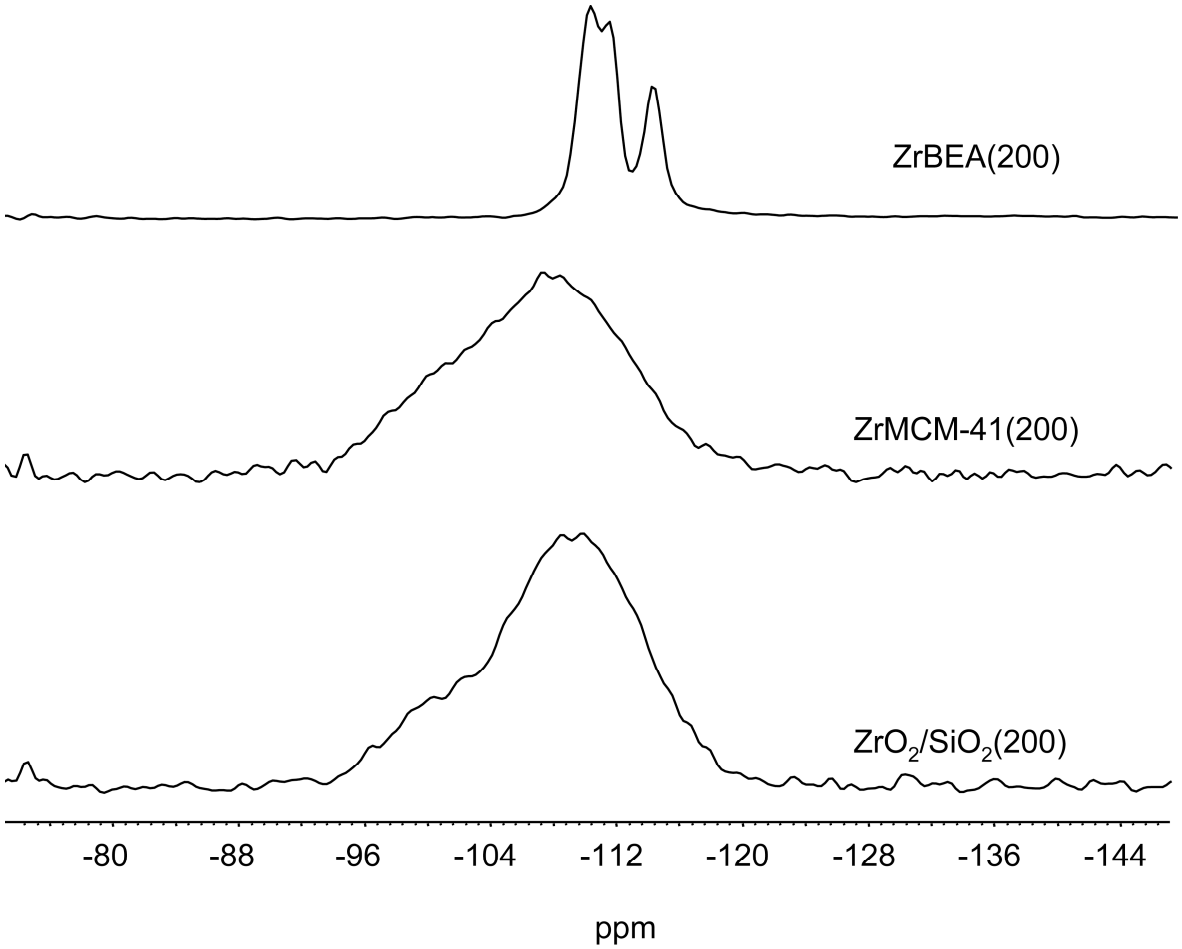

Fig. 4.

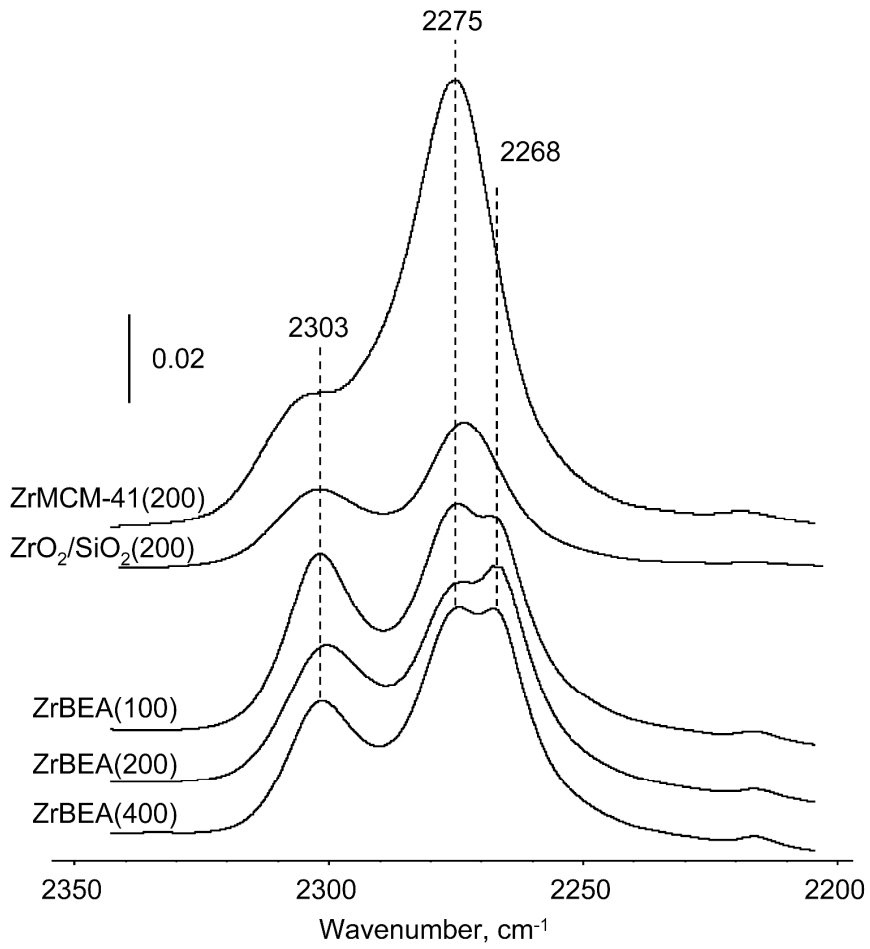

Fig. 5

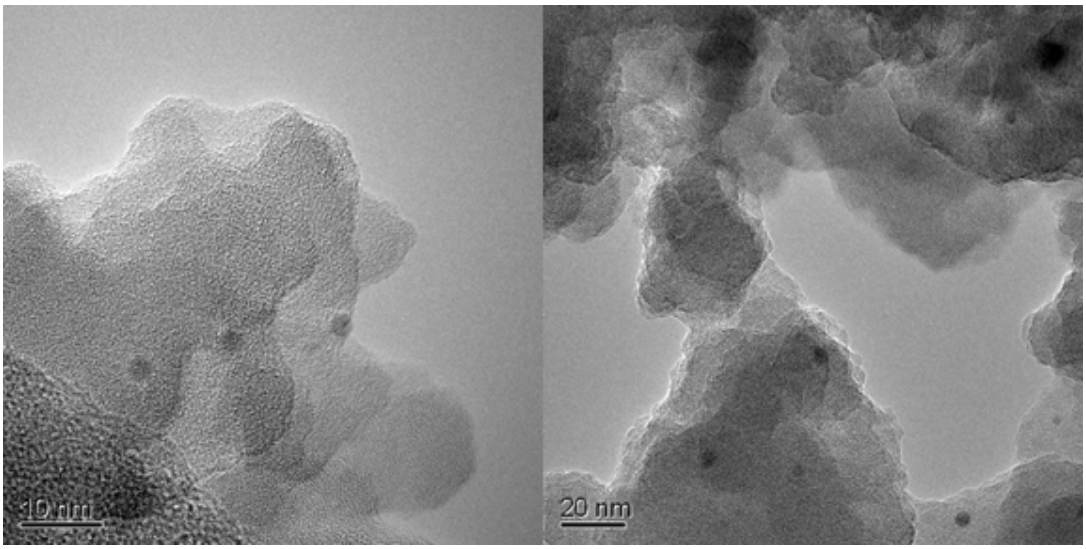

Fig. 6

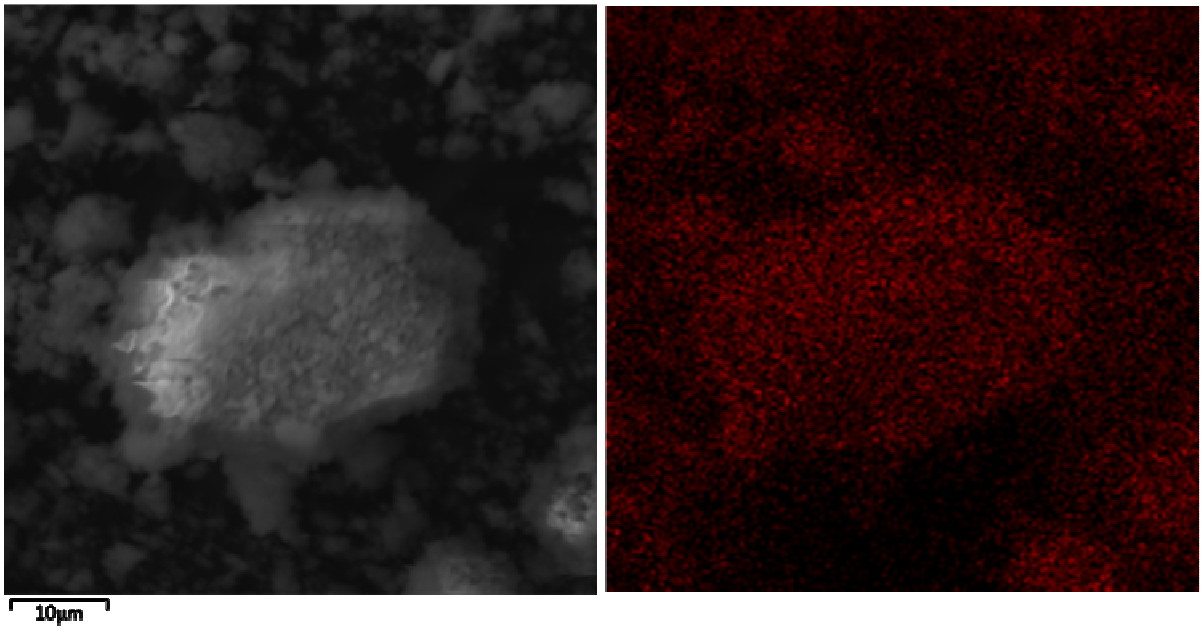

Fig 7.

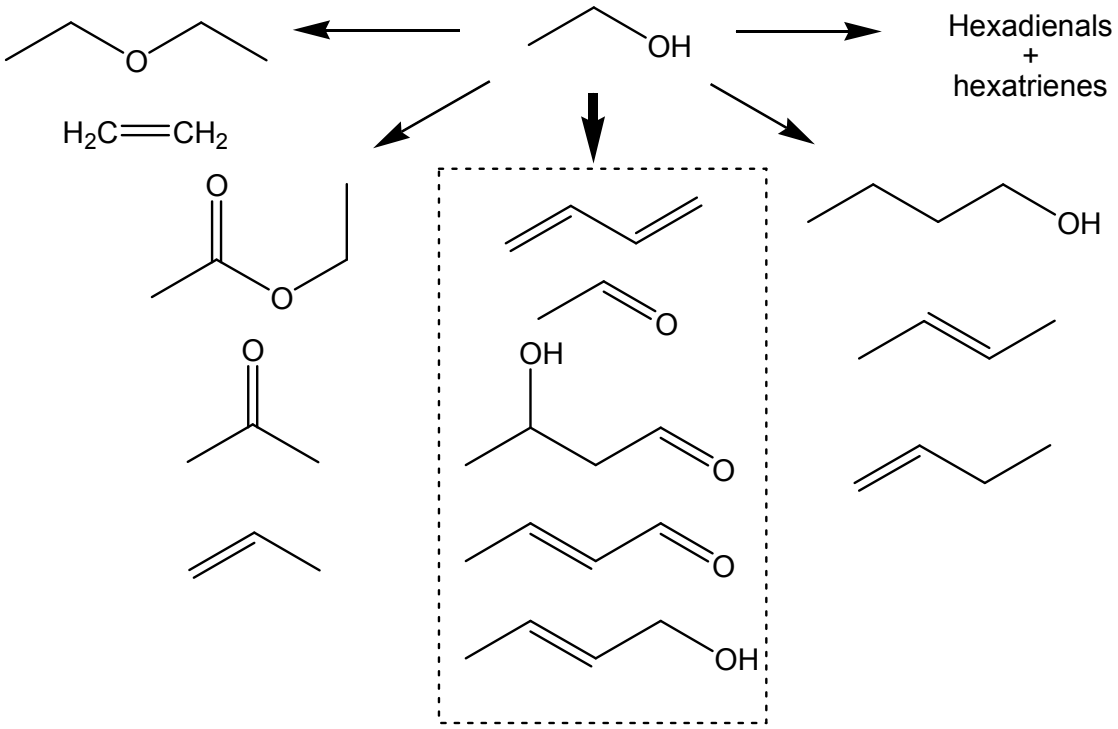

Fig. 8

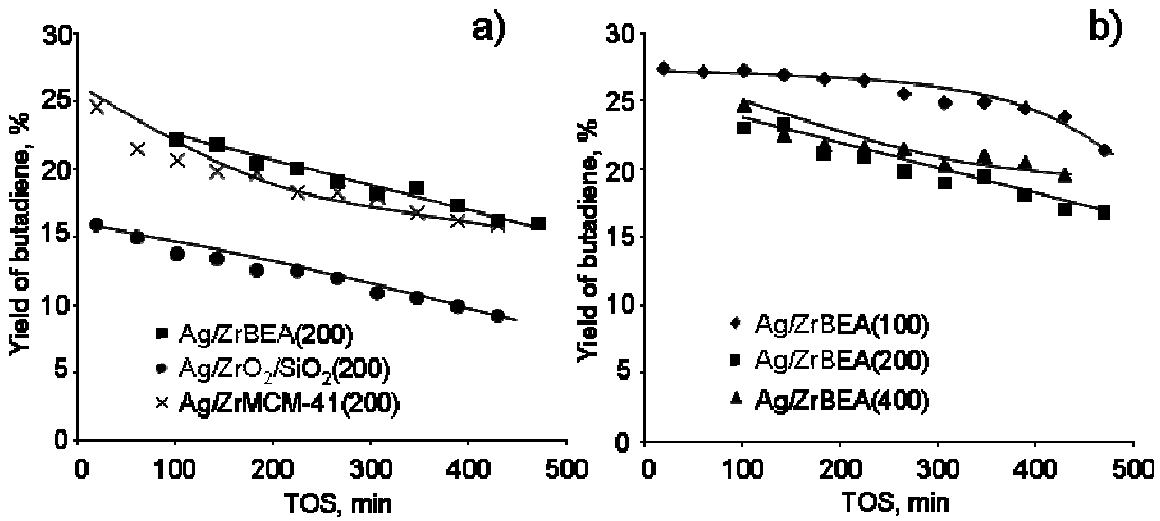

Fig. 9

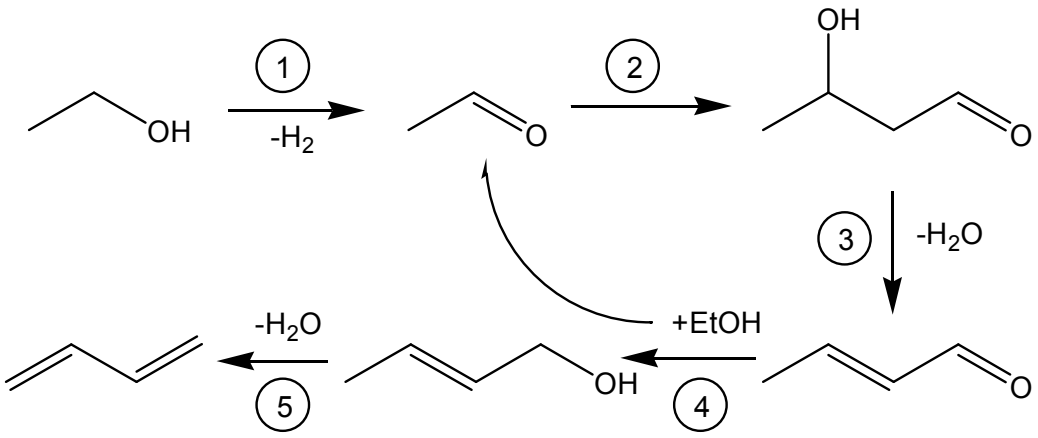

Scheme 1

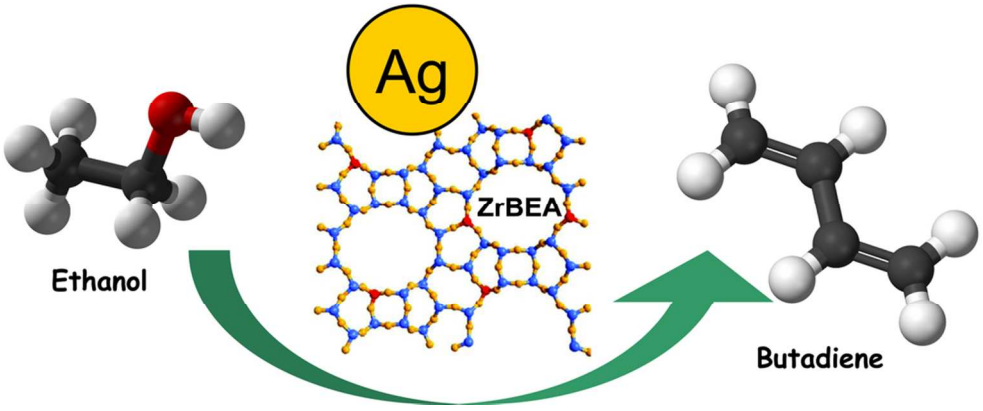

93x37mm (300 x 300 DPI)